

COVER PAGE

Document downloaded by @DAEL

Thu Nov 26 19:30:55 2026
For personal use

When automatic English translation is provided, only the original document is authentic.
The EAA cannot be held responsible of any translation error

Bibliographical reference

Near Infrared Photoacoustic Detection of Heptane in Synthetic Air, Lars Duggen, Mihaela Albu, Morten Willatzen and Horst-Günter Rubahn, Acta Acustica **vol. 99** (Number 2), 2013, pp. 317-322

DOI
https://doi.org/10.3813/AAA.918613

Acta Acustica united with Acustica
Vol. 99 (2013) 317 – 322

DOI 10.3813/AAA.918613

Near Infrared Photoacoustic Detection of Heptane in Synthetic Air

Lars Duggen, Mihaela Albu, Morten Willatzen, Horst-Günter Rubahn
NanoSYD, Mads Clausen Institute, University of Southern Denmark. duggen@mci.sdu.dk

Summary
Trace contaminations of n-heptane in synthetic air is measured in the parts-per-billion (ppb) range using near infrared photoacoustic detection. We describe the fundamental theory used in the design of the photoacoustic cell for trace gas analysis and determine the detection limit of the cell. On the basis of a modified procedure from the American Clinical and Laboratory Standards Institute for the case that it is practically impossible to produce perfectly blank samples, a residual detection limit of 3 ppm n-heptane is confirmed. We investigate theoretically the impact of changing the buffer diameter on the window generated signal and find good correlation with previously reported experimental results.

PACS no. 43.20.Gp, 43.20.Ye, 42.62,Fi

1. Introduction

Detection of trace gases is of great interest in numerous areas. Examples include atmospheric chemistry, studies of volcanic activity, agriculture, monitoring industrial processes and workplace surveillance, and biomedical applications [1, 2, 3]. Considering a wide gamut of application areas, multiple requirements are imposed on the development and implementation of the gas sensors as versatile analytical tools. Partly due to its advantages including a comparably cheap and simple setup with high sensitivities, infrared photoacoustic (PA) spectroscopy is nowadays a widely adopted technique for trace gas detection.

The first PA trace gas detection in the ppm range was reported by K.F. Luft [4] using a differential measurement principle in 1943. In the follow the PA detection of gas traces has been studied most intensively in the 1970s and 1980s [5], both due to the increasing availability of laser sources and the thorough theoretical treatment by Rosencwaig and Gersho[6, 7]. It started with the initial work of Kreuzer [8] who was able to detect heptane concentration down to 10^{-8} with a 15 mW Helium-Neon laser, using a PA cell operated at a non-resonant modulation frequency. This was further extended by Dewey *et al.* [9] who used a resonant cell design to amplify the acoustic signal by a factor of 100. These measurements showed the low-concentration measurement properties of the PA technique, being able to measure absorption levels (i.e. lower pollutant concentrations) considerably lower than gross methods like laser transmission monitoring [10]. This was followed by the use of CO_2 lasers with considerably higher output power at $\sim$ 1W. With this type of laser, Kreuzer *et al.* [11] managed to push the detection limit of ethylene to 0.3 ppb and other pollutants as NO and NO_2 in the low ppb range. Indeed, if placing the PA cell in the optical cavity of the CO_2 laser the intensity of the irradiation can be significantly increased [12, 13] and a high sensitivity can be reached. Thus, Harren *et al.* [13] reported a sensitivity of 6 ppt (parts per trillion) of C_2H_4. Nowadays, usually CO or CO_2 lasers with an output energy of $\sim$ 10 W are employed [5]. Despite the large dimensions and difficult handling, Sigrist *et al.* [14, 15] managed to use such a setup for in vivo measurements of pollutants in atmospheric air – in urban environments.

Still, a CO_2 laser is not a convenient choice as a source in many applications, where size is an important, if not critical, factor. When space is a crucial factor, one has to choose other excitation sources such as diode lasers or quantum cascade lasers [16].

In addition to the improvement of laser sources, also the detection methods have been studied, and still are of significant interest. In addition to a usual microphone [10], cantilever microphone setups [17, 18], electroactive polymer transducers [19], and, more recently, small scale piezoelectric tuning forks (QEPAS) [20] have been employed successfully.

The PA effect is based on the heat generation by absorption of light. When the light source is amplitude modulated, the corresponding generated heat will be amplitude modulated as well. Since a change in local temperature causes a change in local pressure the modulated light source will generate an acoustic field. The amplitude of the sound wave resulting from the pressure fluctuations is directly proportional to the concentration of the gas and can be detected by a microphone in combination with a lock-in amplifier [12, 21]. A simplified sketch of the PA setup can be seen in Figure 1.

Received 24 May 2012,
accepted 3 December 2012.

© S. Hirzel Verlag · EAA

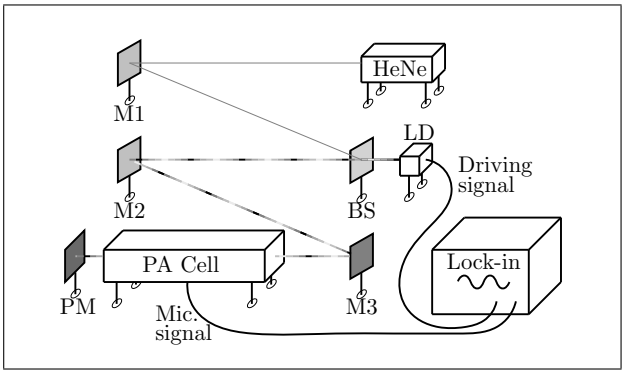

Figure 1. Sketch of the employed PA setup. M1, M2, and M3 are mirrors, while BS denotes a beam splitter and LD is a laser diode. After the PA cell we have placed a power meter (PM) for reference. For clarity, we chose not to show lenses for focusing the laser beams here.

We describe the fundamental theory and its usage for designing a PA cell and report the feasibility of near infrared light sources for detection of heptane in synthetic air. For this purpose we use a modified procedure for calculation of the detection limit, as blank samples are impossible to create in this case. As mixtures of synthetic air and n-heptane share significant infrared absorption properties with synthetic air polluted by widely used oil types, we expect that our analysis and methodology can be extended to oil polluted pressurized air, as commonly found in industrial applications.

2. Theory

The fundamental equations for the generation and propagation of a PA signal read [22]

$$\rho_0 \frac{\partial \mathbf{u}}{\partial t} = -\nabla p + \left(\eta + \frac{4}{3}\mu\right)\nabla\nabla\cdot\mathbf{u} - \mu\nabla\times\nabla\times\mathbf{u}, \tag{1}$$

$$\frac{\partial \delta\rho}{\partial t} + \rho_0 \nabla\cdot\mathbf{u} = 0, \tag{2}$$

$$\rho_0 T_0 \frac{\partial \sigma}{\partial t} = \kappa\nabla^2\tau + \sigma_{abs}\epsilon. \tag{3}$$

In the above equations, $\mathbf{u}, p, \rho, \tau$ and σ denote particle velocity, pressure, mass density, temperature and entropy, respectively, while $\eta, \mu,$ and κ denote bulk and shear viscosity and heat transfer coefficients, respectively. Finally the term σ_{abs} is the absorption cross section with ϵ being the intensity of the irradiation source, in other words $\sigma_{abs}\epsilon$ is the driving heat source, being the inhomogeneous term in the heat-flux continuity equation. We have split the thermodynamic quantities into constant background and acoustic contributions as

$$\begin{aligned} \mathbf{U} &= \mathbf{u}_0 + \mathbf{u}, \quad P = P_0 + p, \quad \rho = \rho_0 + \delta\rho, \\ T &= T_0 + \tau, \quad S = \sigma_0 + \sigma, \end{aligned} \tag{4}$$

where the left hand side terms are total quantities, the first terms of the right hand side are equilibrium quantities and the last terms are the fields generated by the irradiation. In the above equations we have assumed that there is no background flow, i.e. $\mathbf{u}_0 = 0$ as this reduces $d/dt \to \partial/\partial t$. Further manipulation, assuming cylindrical symmetry and harmonic excitation, allows us to simplify the governing equations to a Helmholtz equation for the propagational mode,

$$\nabla^2 p + k^2 p = -\mathrm{i}\omega\frac{\alpha\gamma\sigma_{abs}\epsilon}{\rho C_p c^2}, \tag{5}$$

where C_p is the constant pressure heat capacity and c is the speed of sound in the medium. The thermal mode is accounted for in the boundary conditions, reading [23]

$$\frac{\partial p}{\partial r}\bigg| r_R = \mathrm{i}\omega\rho_0\left[\frac{1}{z} - \frac{\mathrm{i}+1}{\rho_0 c}\left((\gamma-1)\frac{J_1\left(\sqrt{\frac{\mathrm{i}\omega}{l_h c}}R\right)}{J_0\left(\sqrt{\frac{\mathrm{i}\omega}{l_h c}}R\right)}\sqrt{\frac{l_h\omega}{2c}} + \frac{k_t^2 c^2}{\omega^2}\frac{J_1\left(\sqrt{\frac{\mathrm{i}\omega}{l_v c}}R\right)}{J_0\left(\sqrt{\frac{\mathrm{i}\omega}{l_v c}}R\right)}\sqrt{\frac{l_v\omega}{2c}}\right)\right]p, \tag{6}$$

where z, J_n, k_t denote the acoustic impedance of the wall material, the n-th order Bessel function, and the transverse wavenumber (see discussion in [23, 22]), respectively. Furthermore, l_h, l_v denote thermal and viscous loss terms given by

$$l_h = \frac{\kappa}{\rho_0 C_p c}, \tag{7}$$

$$l_v = \frac{\mu}{\rho_0 c}. \tag{8}$$

In principle one also needs to adjust the above source term to include the driving term from the thermal part (using the thermal expansion coefficient, see [10]), but as we are doing a qualitative analysis, the amplitude of the source term is of negligible importance. We solve the non-homogeneous Helmholtz equation with a non-separable geometry using the Finite Element Method (FEM) in two dimensions, saving a significant amount of computation time compared to a three dimensional analysis. FEM approaches similar to ours, just with simplified boundary contitions, have been employed with some success before [24, 25, 26], however not predicting Q-factors.

A solution with the above boundary conditions gives us a qualitative prediction of how the cell performs in terms of quality factor [23] and influence of window noise, with the latter being an acoustic signal generated by infrared absorption of the window materials. Both induced pressure and temperature changes couple into the gas sample area and give rise to a background signal of the same frequency as the main signal.

3. Experimental Setup

The experimental setup for the PA detection of n-heptane in synthetic air consists of a light source, a PA cell and

signal acquisition and processing equipment. An overall schematic of the experimental setup is presented in Figure 1. The synthetic air is a gas mixture of 21% oxygen and 79% nitrogen with a purity of 99.999% (SA 5.5 from Yara Praxair). We consider this to be the best option to simulate air pressure systems in a controllable lab environment. Using mass flow controllers in a gas mixing unit, sketched in Figure 2, controlled levels of n-heptane (HPLC grade, from Rathburn Chemicals Ltd. – Walkerburn, Scotland, UK) were injected in the PA cell. We started with reasonably high concentration, in the high *ppm* range, and used a calibrated commercial instrument, 1314 Photoacoustic Multi-gas Monitor from Innova Air Tech Instrumennts, to determine the level of n-heptane. In Figure 2 this first step corresponds to the lower pipe path, where pressurized synthetic air (1bar) is going through the n-heptane bottle. The n-heptane was introduced using a bubbler at room temperature, where the air flow rate was kept constant until the Innova Air reference device gave stable results for at least ten measurements. This gas mixture contains virtually only n-heptane.

In addition to injecting this mixture into the PA cell and reading with the Innova Air reference instrument, we lead it back into the dilution loop. For that, the valve to the lower path, used to start, is closed and the pressure is increased by adding more synthetic air. By increasing the pressure, only adding synthetic air, the n-heptane concentration in the mixture is scaled proportionally. This air mixture is subsequently partially released to obtain a pressure of 1bar. This dilution procedure is repeated over and over in order to obtain very low concentration samples. The precision of this technique is limited mainly by the precision of the manometers. As the manometers we used are of analog type, their precision is rather limited by output resolution (reading the analog scale) and should lie in the low percentage range – therefore the same applies to the precision of our dilution technique.

The infrared light source is a distributed feed-back laser diode FLO-950 (300 mW, $\lambda = 1725$ nm, $\delta\lambda = 5$ nm) based on a GaInAsP/InP quantum well structure semiconductor laser from Frankfurt Laser Company. The optical properties and the high output power of the laser diode allow for an advanced collimation in order to correct for beam divergence. A He-Ne laser was used to simplify the alignment procedure. The divergence of the aligning laser was adjusted by means of a lens and via a beam splitter brought to overlap with the beam of the laser diode. An additional lens was used to produce a focus of the laser diode inside the PA cell to obtain full control over the beam propagation. The focus diameter inside the PA cell results in 95% power transmittance through an aperture of approximately 1 mm.

The opto-mechanical setup, was operated at 1250 mA and 15°C; the output power of the laser was 110 mW. The laser beam traverses the PA cell containing the gaseous sample; the position of the focus coincides with the location of the microphone in the PA cell.

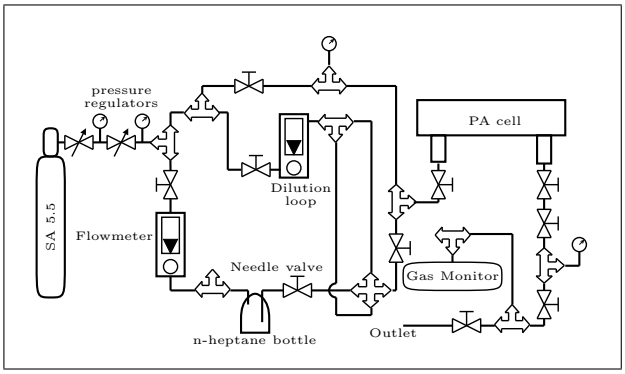

Figure 2. Schematic of the setup for creation of sample mixtures.

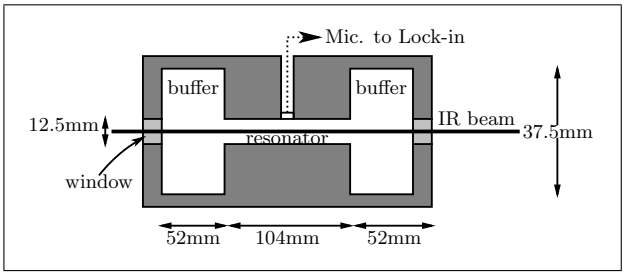

Figure 3. Cross section of a widely used cylindrical PA cell geometry [29]. The thick line in the middle represents the laser beam while the light-gray areas depict BK7 windows.

The geometry of the PA cell is of great importance and was designed using the theoretical model described in section 2. The cell is of resonant type operating in its first longitudinal mode at ~ 1.65 kHz. The dimensions of the PA cell are depicted in Figure 3. The PA cell was constructed from a gold-coated stainless steel block and closed by means of two high precision windows (BK 7) provided with the anti reflection coating.

To generate a PA signal, the intensity of the laser is sinusoidally modulated. The signal detected by the microphone is therefore phase and amplitude correlated to the gas concentration, as well as average power and modulation depth of the infrared laser light. To modulate the laser power, the diode current was modulated via a laser diode driver. The signal source for the modulation was taken from the internal sine generator of the lock-in amplifier.

The average laser power was set directly on the laser driver. A TEC-temperature PID controller was used to stabilize the wavelength of the laser diode. The PA signal is detected by a fibre optical microphone Optimic 4110FA from Optoacoustics. The microphone has a sensitivity of 5 V/Pa @ 1.65 kHz. The electrical signal is furthermore filtered and amplified with a Kemo BenchMaster 8.41 filter/amplifier unit with an adjustable band pass filter (8 pole Butterworth filter -48 dB/octave) from Kemo Limited. The refurbished signal was connected to a lock-in amplifier (model SR 830 from Stanford Research Systems) to extract the correlated fraction of the signal.

The data was send to a PC via serial communication over the RS-232 port and interpreted by a LabVIEW based data acquisition software.

Measurements were performed on n-heptane (C_7H_{16}) in synthetic air (SA, 5.5) at room temperature and atmospheric pressure resulting in a sound velocity of $c = 343\,\mathrm{m/s}$. Due to vibrational transitions of the methylene (CH_2) and the methyl (CH_3) groups, absorption bands of n-heptane are located in the spectral region around $1.7\,\mu\mathrm{m}$ [27, 28]. No interfering absorptions of atmospheric gases such as carbon dioxide (CO_2) and water (H_2O) occur in this spectral regime.

The PA spectra of various mixtures of n-heptane in synthetic air at atmospheric conditions were recorded by scanning the stimulus laser modulation frequency between 1300 and 1800 Hz.

4. Data Analysis

The data measured using the above experimental setup are normalized with respect to the microphone response and the resulting acoustic frequency spectrum is fitted to a Lorentzian curve, with the amplitude of the best fit being the indicator for heptane concentration. According to the datasheet of the microphone, the frequency response is increasing almost linearly with a slope of $3/2500$ dB/Hz up the maximum response at 1650 Hz. Then it decreases linearly with a slope of $3/1500$ dB/Hz. Thus we obtain the corrected amplitude A in terms of the measured amplitude A_{meas} at frequency f by

$$A(f) = \begin{cases} A_{meas} \cdot 10^{\frac{3}{2500}\cdot(1650-f)} & \text{for } f \leq 1650, \\ A_{meas} \cdot 10^{\frac{3}{1500}\cdot(f-1650)} & \text{for } f \geq 1650. \end{cases} \quad (9)$$

The results from each frequency scan were analysed with respect to signal amplitude using a Lorentzian curve fit as described in [30]. This curve fitting will yield an estimate for the amplitude of the signal which we can correlate to the measured heptane concentration. We use these measurements as a basis for the calculation of the detection limit. The definition of the limit of detection (LoD) we use is taken from the guidelines of the American Clinical and Laboratory Standards Institute [31]. These guidelines introduce both the LoD, the limit of blank (LoB), and the limit of quantification (LoQ), of which only the former two are of interest for us. The LoB denotes the maximum measured concentration using blank samples, i.e. it is an indicator of the absolute error at extremely low concentrations. The LoD on the other hand, denotes the concentration which can be reliably distinguished from blank samples. The reliability is determined by a chosen confidence interval (we use 95%), stating the statistic fraction of correctly distinguished samples. For finding the LoD, we start by finding the LoB, which is given by

$$LoB = \mu(C_{blank}) + 1.645 \cdot \sigma(C_{blank}), \quad (10)$$

where μ denotes the mean value, σ the standard deviation of the measured blank sample concentrations C_{blank}, and the factor 1.645 corresponds to a confidence interval of 95%. As it is practically impossible to create perfectly blank samples, mainly due to small contaminations in synthetic air, we block the laser before entrance to the cell and measure the noise level. This we compare to the signal without blocking the laser C_{low}, with the mean value of the difference describing the window signal C_{win}. Eventually we add this C_{win} to the LoB in order to obtain a LoB that includes the generated window signal, thus

$$LoB \rightarrow \mu(C_{blank}) + C_{win} + 1.645 \cdot \sigma(C_{blank}). \quad (11)$$

The LoD is then found by

$$LoD = LoB + 1.645 \cdot \sigma(C_{low}). \quad (12)$$

Note that the values of $C_{blank}, C_{win}, C_{low}$ still are amplitude values of the curve fitting and have to be mapped to a corresponding heptane concentration. This bijective map is a simple linear scaling, where we use higher concentration measurements carried out earlier [30] to find the slope of amplitude vs. concentration and we use the background measurements to find the offset. The higher concentration measurement results, in terms of fitted amplitude A can be seen in Figure 6.

5. Results

Besides the prediction of Q-factor [23, 30] the mathematical model also gives the opportunity to investigate the influence of window absorption signals to the measured signal. Here we simply used a thermal piston approximation [6] and simulated the acoustic behaviour with and without these thermal pistons applied as boundary conditions. As we want to match the resonance of the microphone, we have already determined the length of the resonator section, with the diameter miniaturisation being limited by the focus of the laser beam. The length of the buffer was, as usual [32], fixed to half of the resonator length as to correspond to a $\lambda/4$ filter to reduce the influence of the window signal. The results of the buffer diameter sweep are shown in Figure 4. Again, as we do a qualitative analysis, the absolute value of the signal to background ratio is arbitrary.

As we can see, the increase of the buffer diameter is effective only up to a certain maximum diameter. In our case, since we have to consider electronic noise due to the very low absolute signal magnitude, we have chosen a ratio of three, where the slope of increasing filter functionality starts to decrease significantly. It should be noted that these results correspond to the experimental observations made by Bijnen *et al.* [33], who used a resonator radius of 3 mm and found that the slope of the window signal strength decreased from an average ~ -0.05 mPa/W/mm at a buffer radius between 6 and 10 mm over ~ -0.025 mPa/W/mm between 10 and 15 mm down to ~ -0.001 mPa/W/mm above 15 mm (values estimated from Figure 2d, [33]).

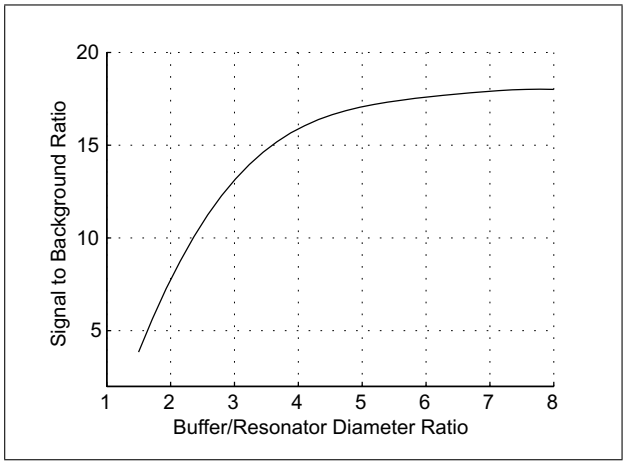

Figure 4. Influence of window signal. The resonator length is fixed to 104 mm while the buffer length is fixed to half of that. The resonator diameter is fixed to 12.5 mm and the buffer diameter is varied, yielding different buffer/resonator diameter ratios. The excitation frequency is 1670 Hz.

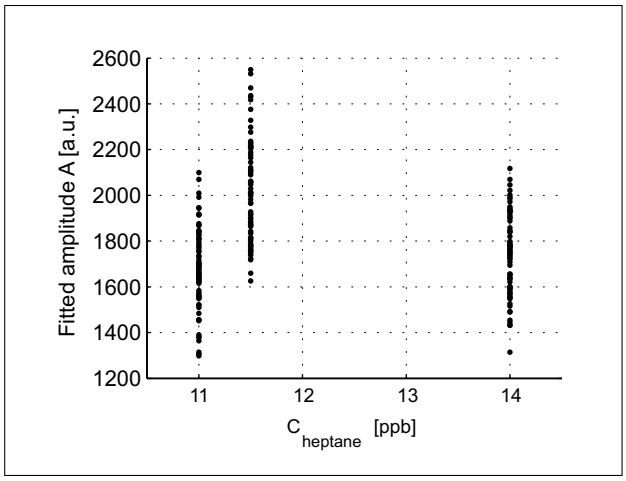

Figure 5. Measurement results from three low-concentration samples prepared by the dilution technique. Analysis of these measurements yield a LoD of 2484, in units of fitted amplitude.

The results of the measurements for the low concentration samples, prepared using the dilution technique, are shown in Figure 5.

We have used three independent samples and recorded all in all 71 frequency sweeps and analysed them by Lorentzian curve fitting. The mean value of the fitted amplitude for the low concentration signals is found to be 2018, with the LoD value being 2484. In order to determine the corresponding concentration we use a different set of measurements where higher concentrations were measured as well [30], see the results on Figure 6.

As these measurements are fairly linear with respect to reference measurements, we use the obtained slope (144 ppm^{-1}) to estimate the LoD being 3 ppm, when using the 95% level of significance.

It should be noted, however, that this detection limit only applies to a well-calibrated device, where measure-

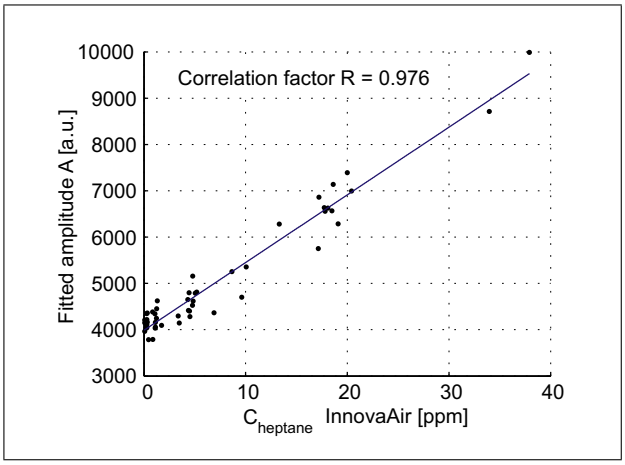

Figure 6. Measured concentrations (in units of fitted amplitude A) vs. concentrations measured by reference device. The measured concentrations are fairly linear with respect to the reference concentrations. Due to different parameters for the curve fitting function (there were several months between the experiments), the A-values from figure 5 and this figure differ in offset.

ments using a blocked laser and very low heptane concentrations (well below the LoD) have been carried out in order to filter background information and determine the window signal. Instead of low heptane concentrations one could also use a different laser wavelength that is not absorbed in the sample gas in order to estimate the magnitude of the window signal.

6. Conclusion

We have used a resonant PA cell to measure n-heptane concentrations in synthetic air. We used FEM to simulate the acoustic cell behaviour, determining the influence of the buffer diameter on the window signal level, and designed the cell accordingly. This cell was used to measure prepared samples of n-heptane contaminated synthetic air. We have described a methodology, based on the guidelines of the American Clinical and Laboratory Standards Institute, how to determine the detection limit of the cell. The guidelines had to be modified to account for the lack of completely blank samples. Using this methodology we find that our PA setup has a detection limit of 3 ppm with 95% confidence level. While we do believe that this setup is already working well, there should be room for some slight improvements. This includes a re-estimation of the cell dimensions, as resonance does not occur exactly at the microphone resonance. The reason for this is a model inaccuracy regarding damping mechanisms. The true cell has a significantly lower Q-factor than predicted, which also causes the resonance of the cell to be lower than predicted.

Acknowledgement

Financial support from the Danish National Advanced Technology Foundation is gratefully acknowledged.

References

[1] A. Elia, P. M. Lugarà, C. Di Franco, V. Spagnolo: Photoacoustic techniques for trace gas sensing based on semiconductor laser sources. Sensors **9** (2009) 9616.

[2] M. Xu, L. V. Wang: Photoacoustic imaging in biomedicine. Review of Scientific Instruments **77** (2006) 041101.

[3] H. F. Zhang, K. Maslov, G. Stoica, L. V. Wang: Functional photoacoustic microscopy for high-resolution and noninvasive in vivo imaging. Nature Biotechnology **24** (2006) 848.

[4] K. F. Luft: Spektroskopie - Über eine neue Methode der registrierenden Gasanalyse mit Hilfe der Absorption ultraroter Strahlen ohne spektrale Zerlegung. Zeitschrift für Technische Physik **24** (1943) 97.

[5] A. Miklos, P. Hess. Analytical Chemistry **72** (2000) 30A.

[6] A. Rosencwaig, A. Gersho: Theory of the photoacoustic effect with solids. Journal of Applied Physics **47** (1976) 64.

[7] A. Rosencwaig: Theoretical aspects of photoacoustic spectroscopy. Journal of Applied Physics **49** (1978) 2905.

[8] L. B. Kreuzer: Ultralow gas concentration infrared absorption spectroscopy. Journal of Applied Physics **42** (1971) 2934.

[9] C. F. Dewey, R. D. Kamm, C. E. Hackett: Acoustic amplifier for detection of atmospheric pollutants. Applied Physics Letters **23** (1973) 633.

[10] A. C. Tam: Applications of photoacoustic sensing techniques. Review of Modern Physics **58** (1986) 381.

[11] L. B. Kreuzer, N. D. Kenyon, C. K. N. Patel: Air pollution: Sensitive detection of ten pollutant gases by carbon monoxide and carbon dioxide lasers. Science **177** 347–349.

[12] W. Demtröder: Laser spectroscopy - Basic concepts and instrumentation. 3rd ed. Springer, Berlin / Heidelberg, Germany, 2003.

[13] F. J. M. Harren, F. G. C. Bijnen, J. Reuss, L. A. C. J. Voesenek, C. W. P. M. Blom: Sensitive intracavity photoacoustic measurements with a CO_2 waveguide laser. Applied Physics B **50** (1990) 137–144.

[14] M. W. Sigrist, A. Thony: Atmospheric trace gas monitoring by CO_2 laser photoacoustic spectroscopy. Proceedings of SPIE **1715** (1992) 174.

[15] P. L. Meyer, M. W. Sigrist: Atmospheric pollution monitoring using CO_2 laser photoacoustic spectroscopy and other techniques. Review of Scientific Instruments **61** (1990) 1779.

[16] M. W. Sigrist: Trace gas monitoring by laser photoacoustic spectroscopy and related techniques (plenary). Review of Scientific Instruments **74** (2003) 486.

[17] J. Kauppinen, K. Wilcken, I. Kauppinen, V. Koskinen: High sensitivity in gas analysis with photoacoustic detection. Microchemical Journal **76** (2004) 151.

[18] K. Wilcken, J. Kuppinen: Optimization of a microphone for photoacoustic spectroscopy. Applied Spectroscopy **57** (2003) 1087.

[19] A. Manninen, J. Sand, J. Saarela, T. Sorvajärvi, J. Toivonen, R. Hernberg: Electromechanical film as a photoacoustic transducer. Optics Express **17** (2009) 16994.

[20] A. A. Kosterev, Y. A. Bakhirkin, R. F. Curl, F. K. Tittel: Quartz-enhanced photoacoustic spectroscopy. Optics Letters **27** (2002) 1902.

[21] K. H. Michaelian: Photoacoustic infrared spectroscopy. Wiley-Interscience, Hoboken, NJ, 2003.

[22] P. M. Morse, K. U. Ingard: Theoretical acoustics. Princeton University Press, Princeton, NJ, 1986.

[23] L. Duggen, N. Lopes, M. Willatzen, H.-G. Rubahn: Finite element simulation of photoacoustic pressure in a resonant photoacoustic cell using lossy boundary conditions. International Journal of Thermophysics **32** (2011) 774–785.

[24] M. Wolff, H. Groninga, B. Baumann, B. Kost, H. Harde: Resonance investigations using PAS and FEM. Acta Acoustica united with Acustica **99** (2005) Suppl. 1.

[25] B. Baumann, M. Wolff, B. Kost, H. Groninga: Finite element calculation of photoacoustic signals. Appl. Opt. **46** (2007) 1120–1125.

[26] B. Baumann, B. Kost, H. Groninga, M. Wolff: Eigenmode analysis of photoacoustic sensors via finite element method. Review of Scientific Instruments **77** (2006) 044901.

[27] V. Vesnin, V. Muradov: Isosbestic points in absorption spectra of isooctane, n-heptane, toluene, and benzene binary mixtures. Journal of Applied Spectroscopy **76** (2009) 641–645.

[28] J. J. Kelly, J. B. Callis: Nondestructive analytical procedure for simultaneous estimation of the major classes of hydrocarbon constituents of finished gasolines. Analytical Chemistry **62** (1990) 1444–1451.

[29] E. Nodov: Optimization of resonant cell design for optoacoustic gas spectroscopy (h-type). Appl. Opt. **17** (1978) 1110–1119. http://ao.osa.org/abstract.cfm?URI=ao-17-7-1110.

[30] L. Duggen, M. Albu, M. Willatzen, H.-G. Rubahn: Modelling frequency response of photoacoustic cells using fem for determination of n-heptane contamination in air: Experimental validation. Proceedings of the 4th International Multi-Conference on Engineering and Technological Innovation **2** (2011) 122.

[31] D. A. Armbruster, T. Pry: Limit of blank, limit of detection and limit of quantitation. Clin. Biochem. Rev. **29** (2008) Suppl(i), S49.

[32] A. Miklos, P. Hess, Z. Bozoki: Application of acoustic resonators in photoacoustic trace gas analysis and metrology. Review of Scientific Instruments **72** (2001) 1937.

[33] F. Bijnen, J. Reuss, F. Harren: Geometrical optimization of a longitudinal resonant photoacoustic cell for sensitive and fast trace gas detection. Review of Scientific Instruments **67** (1996) 2914.